Gain dispersion for dissipative soliton generation in all-normal-dispersion fiber lasers

L. M. Zhao,[1,3,*] C. Lu,[1] H. Y. Tam,[2] P. K. A. Wai,[1] and D. Y. Tang[3]

[1]Department of Electronic and Information Engineering, Hong Kong Polytechnic University, Hung Hom, Hong Kong, China

[2]Department of Electrical Engineering, Hong Kong Polytechnic University, Hung Hom, Hong Kong, China

[3]School of Electrical and Electronic Engineering, Nanyang Technological University, Singapore 639798

*Corresponding author: luming_zhao@pmail.ntu.edu.sg

Received 17 June 2009; revised 19 August 2009; accepted 26 August 2009; posted 31 August 2009 (Doc. ID 112994); published 11 September 2009

Properties of dissipative solitons generated in all-normal-dispersion fiber lasers through the gain dispersion effect are numerically studied by using a pulse-tracing technique that considers interaction between gain saturation, gain dispersion, cavity dispersion, fiber Kerr nonlinearity, and cavity boundary conditions. The numerical results qualitatively match with experimental observations and show that the finite gain bandwidth, together with the pump power, determines the properties of the generated dissipative solitons, which further dictates the performance of the pulse compression.

OCIS codes: 060.5530, 060.3510, 140.7090.

1. Introduction

Fiber lasers, as a promising alternative to bulk solid-state lasers, have attracted considerable attention [1]. Apart from alignment-free operation and excellent spatial mode quality, fiber lasers provide other advantages such as compact structure, low cost, and flexibility. Erbium-doped fiber (EDF) lasers are widely used to generate radiation at the telecommunication wavelength window of 1.55 μm, where the availability of fiber-based components from the telecommunication industry accelerates the applications of fiber lasers.

Different from the pulse propagation in conservative systems, due to the existence of a gain-loss mechanism in lasers, pulses generated from the passively mode-locked fiber lasers are generally considered as dissipative solitons [2,3]. Traditionally, fiber lasers were operated in the anomalous cavity group velocity dispersion (GVD) regime, where ultrashort pulses are generated due to the balance between the cavity dispersion and fiber nonlinear Kerr effect. However, the pulse energy is limited to a few hundred picojoules. The appearance of stretched-pulse fiber lasers [4] significantly increases the pulse energy of the generated ultrashort pulses [5]. However, the pulse energy is still limited by the nonlinear phase accumulated in the laser. Recent research has revealed that a higher nonlinear phase shift could be tolerated in the normal dispersion regime (NDR) and that the chirped pulses could be generated in fiber lasers operated in the NDR [6–8], where the GVD and the fiber nonlinear Kerr effect play the same role so that no inherently stable pulses can be generated without additional auxiliary mechanisms. With the help of an intracavity saturable absorber mirror, dissipative solitons with narrow bandwidth were obtained in EDF lasers [8]. It is found that the spectral filtering is crucial for the chirped pulse generation in fiber lasers operated in the NDR. Due to the large

0003-6935/09/275131-07$15.00/0

bandwidth of Yb-doped fibers (YDFs), a separated spectral filter is required for chirped pulse generation in YDF lasers [7]. For EDF lasers, the narrow gain bandwidth itself can function as a spectral filter in the laser cavity; thus a so-called "gain-guided soliton" can be generated [6,9]. A discrete spectral filter is essentially different from the spectral filtering caused by the narrow gain bandwidth, where, apart from the spectral filtering lasting the whole length of the gain medium, the strength of the spectral filtering is determined by the intrinsic features of the gain medium and the pump power. The function of a discrete spectral filter on dissipative solitons in NDR has been analyzed for YDF lasers [10–12]. However, no detailed analysis has been done for the gain dispersion (gain bandwidth limitation) effect on the properties of the generated dissipative solitons, especially when femtosecond pulses are required where an external pulse compressor is necessary. In this paper is a numerical study on the properties of dissipative solitons in all-normal-dispersion EDF lasers. It shows that the finite gain bandwidth, combined with the pump strength, determines the performance of the generated dissipative solitons, thus affecting efficient pulse compression required for high-power femtosecond pulse generation.

2. Laser Schematic and Simulation Model

The numerical simulations are based on a conventional ring fiber laser as shown in Fig. 1. The nonlinear polarization rotation technique is used to achieve the self-started mode locking. To this end, two sets of polarization controllers, one made of two quarter-wave plates and the other made of two quarter-wave plates and one half-wave plate, combined with a polarization-dependent isolator, are used to control the polarization state of the light. A segment of EDF is sandwiched between two segments of dispersion-compensated fiber (DCF) to form the laser cavity. All fibers have normal dispersion at the $1.55\,\mu$m wavelength window. The wavelength-division-multiplexing coupler and the output coupler are both made of the DCF.

We used the pulse-tracing technique to simulate the pulse evolution in the fiber laser [13]. Briefly speaking, we start the simulation with an arbitrary weak pulse and let it circulate in the laser cavity until a steady pulse evolution state is established. Whenever the pulse encounters an individual intracavity component except for the fiber segments, we

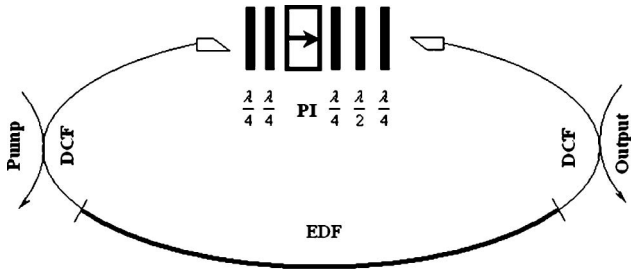

Fig. 1. Schema of fiber laser.

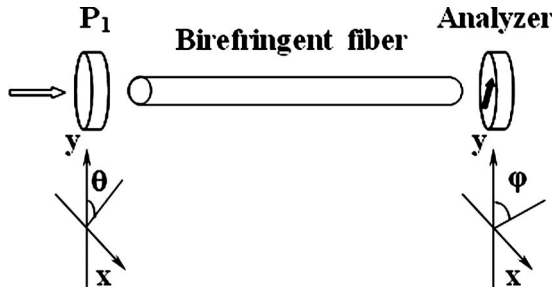

Fig. 2. Equivalent physically simplified laser cavity.

multiply the Jones matrix of the component to the optical field of the pulse. To release the heavy computational requirements, simplification is done for the polarization control section. As shown in Fig. 2, the fiber laser is equivalently simplified into three parts. Polarization controller P_1 at the beginning of the fiber and an analyzer at the end of the fiber describe the roles of the polarization controllers and the polarization-dependent isolator in the fiber laser. The two principal polarization axes of the birefringent fiber are the x (horizontal) and y (vertical) axes, and we consider that the birefringent axes of the three segments of fibers are the same. The fast axis of P_1 and the transmission axis of the analyzer have an angle of θ and ϕ to the y axis of the fiber polarization, respectively.

Starting from a linearly polarized weak pulse F_n, two polarization components are obtained when F_n travels through P_1:

$$\begin{aligned} u &= F_n \sin\theta \exp(i\Delta\Phi), \\ v &= F_n \cos\theta, \end{aligned} \tag{1}$$

where $\Delta\Phi$ is the phase shift between the wave components in the two orthogonal birefringent axes x and y.

Then the two polarization components propagate in the fiber segments, which is governed by the coupled Ginzburg–Landau equations (GLEs):

$$\begin{aligned} \frac{\partial u}{\partial z} &= -i\beta u + \delta\frac{\partial u}{\partial t} - \frac{ik''}{2}\frac{\partial^2 u}{\partial t^2} + \frac{ik'''}{6}\frac{\partial^3 u}{\partial t^3} + i\gamma\left(|u|^2 + \frac{2}{3}|v|^2\right)u \\ &\quad + \frac{i\gamma}{3}v^2u^* + \frac{g}{2}u + \frac{g}{2\Omega_g^2}\frac{\partial^2 u}{\partial t^2}, \\ \frac{\partial v}{\partial z} &= i\beta v - \delta\frac{\partial v}{\partial t} - \frac{ik''}{2}\frac{\partial^2 v}{\partial t^2} + \frac{ik'''}{6}\frac{\partial^3 v}{\partial t^3} + i\gamma\left(|v|^2 + \frac{2}{3}|u|^2\right)v \\ &\quad + \frac{i\gamma}{3}u^2v^* + \frac{g}{2}v + \frac{g}{2\Omega_g^2}\frac{\partial^2 v}{\partial t^2}, \end{aligned} \tag{2}$$

where u and v are the normalized envelopes of the optical pulses along the two orthogonal polarization axes of the fiber, and u^* and v^* are the conjugates of u and v. $2\beta = 2\pi\Delta n/\lambda$ is the wave-number difference between the two polarization modes of the fiber, where Δn is the difference between the effective indices of the two modes, and λ is the wavelength. $2\delta = 2\beta\lambda/2\pi c$ is the inverse GVD, where c is the light speed. k'' is the second order dispersion coefficient, k''' is the third order dispersion coefficient, and γ

represents the nonlinearity of the fiber. g is the saturable gain coefficient of the fiber, and Ω_g is the bandwidth of the laser gain. We note that we take the 3 dB bandwidth throughout the paper if it is not specially stated. Without losing generality, we assume that the peak gain wavelength of the parabolic gain profile coincides with the central wavelength λ_c. For undoped fibers $g = 0$, for EDF, we considered the gain saturation as

$$g = G \exp\left[-\frac{\int(|u|^2 + |v|^2)\mathrm{d}t}{P_{\mathrm{sat}}}\right], \tag{3}$$

where G is the small-signal-gain coefficient and P_{sat} is the normalized saturation energy.

The light propagates along with the laser cavity configuration and finally projects on the transmission axis of the analyzer:

$$F_{n+1} = u' \sin\phi + v' \cos\phi, \tag{4}$$

where u' and v' are the two orthogonal polarization components of the light after propagation in all the fiber segments.

To reveal the properties of the dissipative solitons, we performed numerous numerical simulations under various conditions, varying the gain and gain bandwidth. We assumed that the gain saturation is weak in our simulation. Larger small-signal gain means stronger pump power.

The parameters shown in Table 1 were used for our simulations. L_b is the birefringence beat length, and the laser cavity length $L = 6$ m, which is composed of 1 m DCF, 4 m EDF, and another 1 m DCF in sequence, and the output position is in the middle of the second segment of DCF.

3. Simulation Results

Figures 3(a) and 3(b) show the generated stable dissipative solitons with characteristically steep spectral edges when the small-signal gain is fixed at 1000 and all other parameters are unchanged except the cavity linear phase delay bias (CLPDB) [13], which corresponds to the experimental condition that the pump power is fixed but the wave plates are rotated. We found that, within the mode-locking regime of the CLPDB and with fixed pump power, the spectral bandwidth of the generated dissipative soliton increases with the increasing CLPDB, and simultaneously the temporal pulse width decreases. However, as shown in Table 2, the time–bandwidth product of the generated dissipative soliton is always much larger than that of the transform-limited pulse, which suggests that the generated dissipative soliton is always heavily chirped. Figures 3(c) and 3(d) show a typical operation state obtained in a similar all-normal-dispersion fiber laser [6], where, after a dissipative soliton is experimentally achieved, we only changed the orientation of one of the wave plates while keeping all other operation conditions fixed. Different orientations (marked with letter a, b, and c) correspond to stable dissipative solitons with different properties. Figure 3(c) shows the optical spectrum, while Fig. 3(d) shows the corresponding autocorrelation trace of the stable dissipative solitons. The detailed fiber laser parameters can be retrieved from Ref. 6. A narrower pulse width corresponds to broader spectral bandwidth, which agrees quite well with the simulation result. We note that numerically we obtained a flattop spectrum, and experimentally there was always some structure on the top of the spectrum. We attribute the spectrum difference to the difference between the real gain profile and the numerically assumed parabolic gain profile.

Table 1. Parameters Used in the Simulations

γ	$3\,\mathrm{W^{-1}\,km^{-1}}$	k''_{EDF}	$41.8\,\mathrm{ps^2/km}$
k''_{DCF}	$0.256\,\mathrm{ps^2/km}$	k'''	$-0.131\,\mathrm{ps^3/km}$
L/L_b	2	Ω_g	16 nm
θ	0.152π	φ	$\theta + \pi/2$
P_{sat}	1 nJ	λ_c	1570 nm

Figure 4 shows a typical simulation result obtained when the CLPDB is set at 1.6π and the laser gain is varied, which corresponds to the experimental condition that all the operation conditions are fixed except the pump power. It is obvious that with a fixed CLPDB, both broader spectral bandwidth and wider pulse width are obtained under stronger pump power while the single pulse operation is maintained. This behavior of dissipative solitons has been reported (Fig. 3 in Ref. [6]). The numerical simulation reproduced the experimental observation. Figures 4(c) and 4(d) show the pulse instantaneous frequency (with respect to the central frequency) cross section along the cavity. Since we used the coupled GLEs to simulate the pulse evolution in the cavity to take into account the weak birefringence of the fiber, the instantaneous frequency evolution along each principal birefringence axis is plotted separately. We have overlapped instantaneous frequency profiles at different positions along the cavity in one figure. It is found that not only the instantaneous frequencies of the dissipative solitons along the horizontal and vertical principal axes are almost the same, but also the instantaneous frequencies across the pulse profile at different cavity positions have very small differences. The frequency chirp of the generated dissipative soliton is increased with increasing pump power, and stronger pump power corresponds to faster instantaneous frequency variance.

We also found that the spectral extension of the generated dissipative solitons under increasing pump power is not symmetrically related to the central wavelength as shown in Fig. 4(a). The extension to the short-wavelength side is faster than that to the long-wavelength side. It can be understood as the following: the cavity transmission can be described by [13]

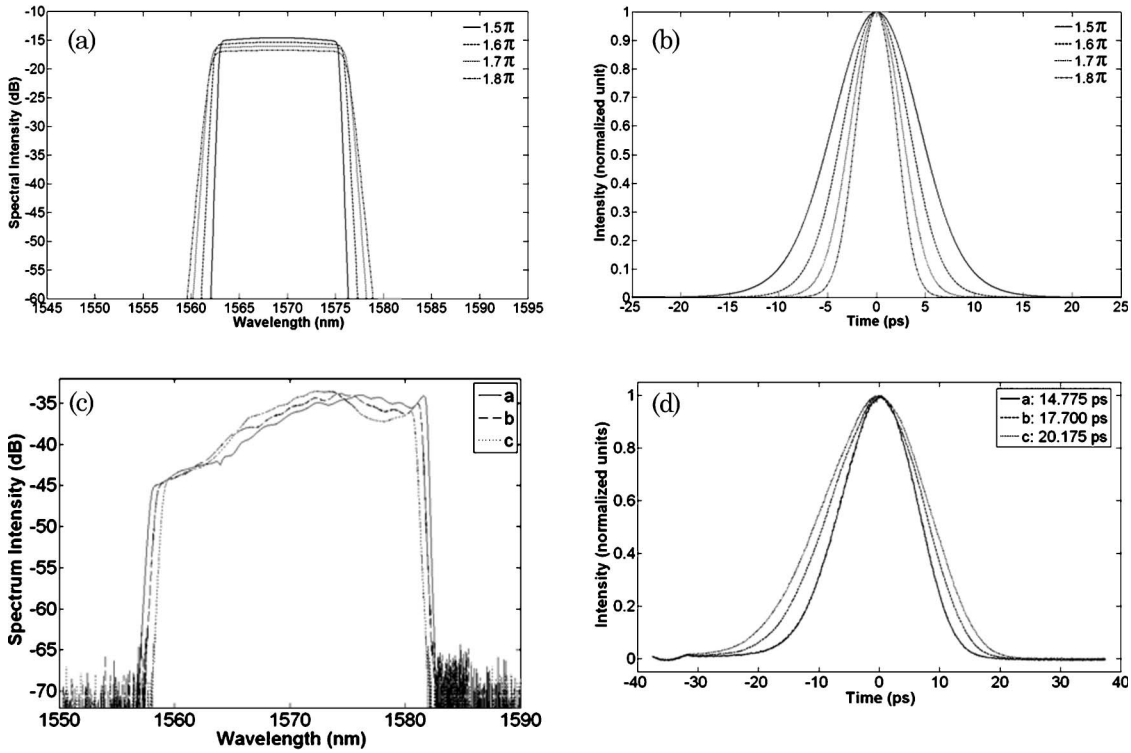

Fig. 3. Dissipative solitons under different CLPDB at $G = 1000$: (a) optical spectrum, (b) autocorrelation trace. Typical experimental results observed: (c) optical spectrum, (d) autocorrelation trace.

$$T = \sin^2\theta \sin^2\varphi + \cos^2\theta \cos^2\varphi + \frac{1}{2} \sin 2\theta \sin 2\varphi \cos[\Phi_l + \Phi_{nl}], \quad (5)$$

where Φ_l is the linear phase delay and Φ_{nl} is the nonlinear phase delay. In the simulation, the linear phase delay includes two parts, the CLPDB and the linear phase shift caused by the fiber birefringence:

$$\Phi_l = \Delta\Phi + 2\pi\left(1 - \frac{\Delta\lambda}{\lambda_c}\right)\frac{L}{L_b}. \quad (6)$$

A simple mathematical calculation shows that, with 1.6π CLPDB, the cavity transmission is monotonously decreased around the central wavelength from the short-wavelength side to the long-wavelength side. As the gain profile is assumed to have a parabolic shape symmetrical to the central wavelength, the effective gain extends further toward the short-wavelength side compared with the long-wavelength side under increasing pump power. Therefore the pulse spectrum extends along both wavelength sides but with further extension at the short-wavelength side compared with the long-wavelength side, and thus the whole pulse spectrum is actually blueshifted with increasing pump power. Determined by the cavity linear phase delay, it is also possible to observe the redshift of the whole pulse spectrum with increasing pump power.

Table 2. Time–Bandwidth Product of the Generated Dissipative Solitons with Different CLPDB and $G = 1000$

CLPDB	1.5π	1.6π	1.7π	1.8π
Spectral bandwidth (THz)	1.547	1.688	1.766	1.766
Pulse width (ps)	10.500	7.906	6.125	4.813
Time–bandwidth product	16.244	13.345	10.817	8.500

The gain bandwidth limitation is crucial for dissipative soliton generation. Numerically once we assume infinite gain bandwidth, no mode locking can be achieved. However, we note that the spectral bandwidth of the generated dissipative soliton can be beyond the gain bandwidth limitation. As shown in Fig. 4(a), the spectral bandwidth is larger than the 16 nm of gain bandwidth when the small-signal gain is larger than 2000. Figure 5(a) shows the spectral bandwidth of the generated dissipative solitons versus the small-signal gain with fixed CLPDB of 1.6π under different gain bandwidth limitation. We found that, after mode locking is achieved, under fixed gain bandwidth limitation and constant CLPDB, there exists an optimal pump value to achieve the maximum spectral bandwidth, which could be larger than the gain bandwidth. We note that we used the 3 dB bandwidth as the pulse spectral bandwidth. Due to the heavier chirp caused by the stronger pump power, a thumblike spectral profile [14] appears as shown in Fig. 5(b), which results in bandwidth reduction with increasing pump power. Too strong a pump power would ultimately destroy the single pulse operation of the fiber laser, and consequently either noiselike pulses [15] or multiple dissipative solitons [16] are obtained.

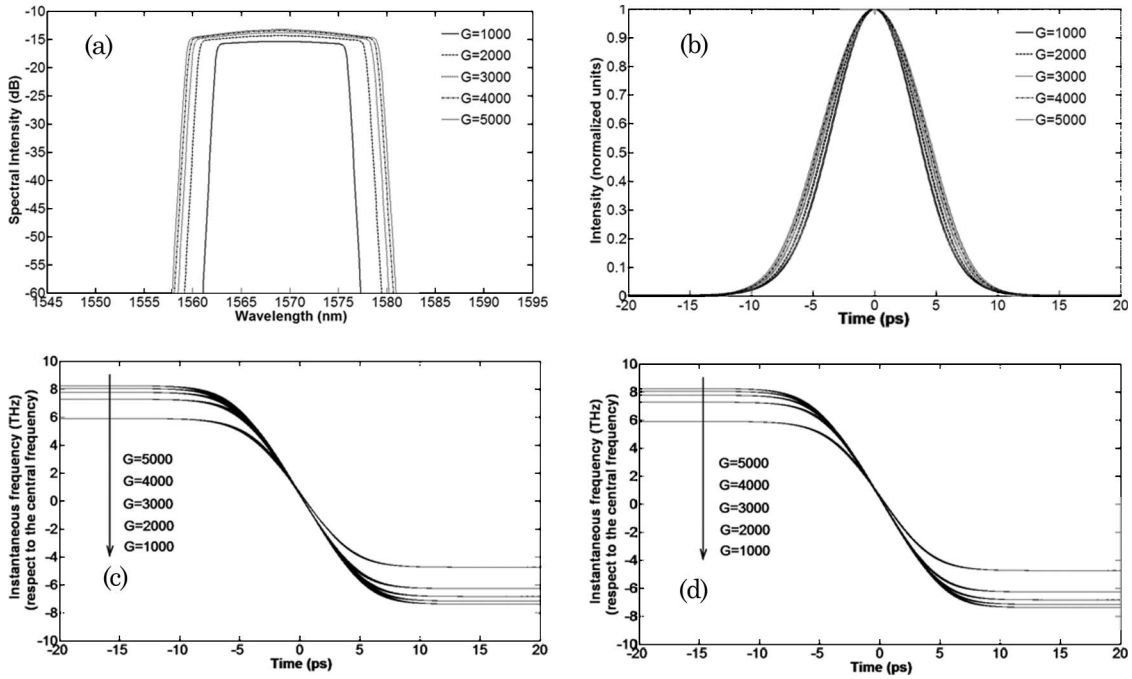

Fig. 4. Dissipative solitons under different small signal gains at CLPDB $= 1.6\pi$: (a) optical spectrum, (b) autocorrelation trace, (c) instantaneous frequency (respect to the central frequency) profiles of the horizontal components at different cavity positions, (d) instantaneous frequency (respect to the central frequency) profiles of the vertical components at different cavity positions.

We have also studied the gain dispersion effect on the properties of the generated dissipative solitons. Figure 6 shows the optical spectra and the temporal profiles of the generated dissipative solitons with the same simulation parameters except the gain bandwidth. The CLPDB is set at 1.6π and the small-signal gain is $G = 1000$. It is clear that the pulse width of the generated dissipative soliton is increased with

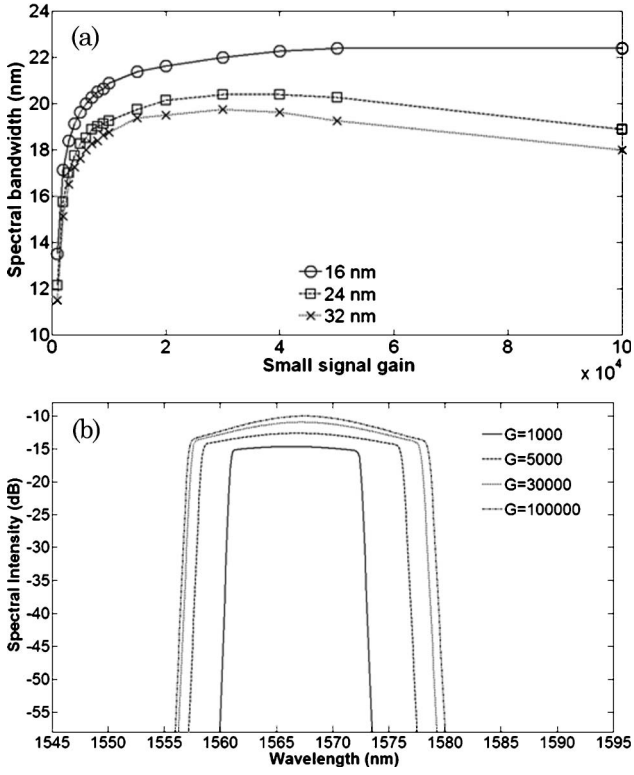

Fig. 5. (a) Spectral bandwidth of the dissipative solitons versus the small-signal gain at CLPDB $= 1.6\pi$ under different gain bandwidth limitations; (b) optical spectrum of the dissipative solitons at CLPDB $= 1.6\pi$ and $\Omega_g = 32$ nm.

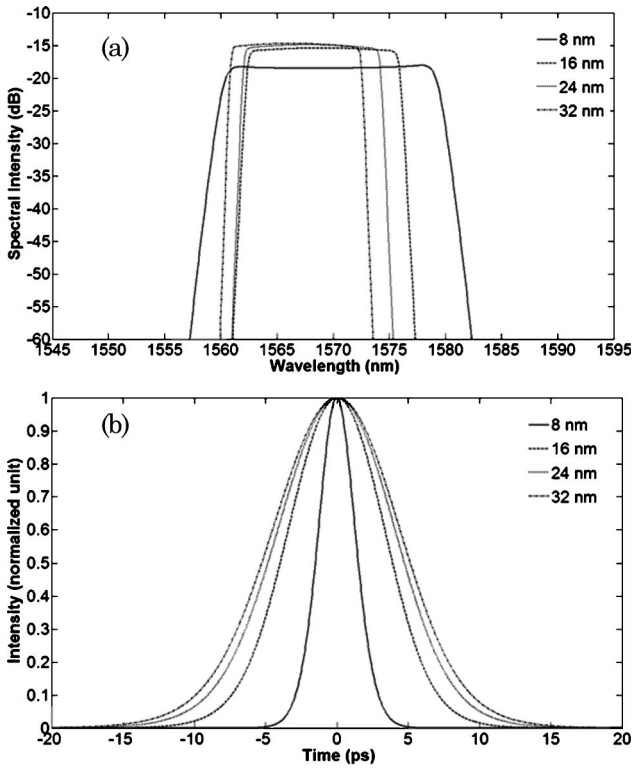

Fig. 6. Dissipative solitons with different gain bandwidths at CLPDB $= 1.6\pi$ and $G = 1000$.

the gain bandwidth, but the spectral bandwidth is reduced. Therefore a gain medium with broader gain bandwidth is favored for large energy pulse generation, as a wider pulse can lower the peak power, consequently reduce nonlinearity, and hence accommodate more energy in the chirped pulses. This conclusion has practical application for YDF lasers, as YDF has broader spectral bandwidth. By using YDF lasers, it is promising to generate pulses with stronger energy compared with the current achievable limitation in YDF lasers with a spectral filter provided that the discrete spectral filter is removed and a stronger pump source is available.

As a dissipative soliton is a heavily chirped pulse, to achieve femtosecond pulses it is necessary to introduce an external pulse compressor. Normally the pulse compressor can be bulky grating pairs or prism pairs. However, due to the anomalous dispersion of standard single mode fibers (SMFs) and the normal chirp of the dissipative solitons, it is naturally possible to use a segment of common fiber to function as the pulse compressor, which has the advantages of no need for alignment, low cost, and simple structure. The nonlinearity of fibers should also affect the dechirp process of the generated dissipative solitons, which is normally ignored when bulky grating pairs or prism pairs are used to compensate the chirp.

Numerically we calculated the pulse evolution in an external segment of SMF with a GVD coefficient of $-20.9\,\mathrm{ps}^2/\mathrm{km}$ beginning from the stable dissipative solitons shown in Fig. 4. Figures 7(a) and 7(b) show the detailed pulse width evolution in a 40-m-long SMF when the fiber nonlinearity is considered and that in a 50-m-long SMF when the fiber nonlinearity is not considered, respectively. Figures 4(c) and 4(d) suggest that the frequency chirp of the generated dissipative soliton is increased with increasing pump power. However, the dechirping process shown in Fig. 7 suggests that the fiber length needed to achieve the minimum pulse width is nearly the same for dissipative solitons with different chirp when the chirp is larger than a certain value. The minimum pulse width after compression is independent of the chirp. Taking the fiber nonlinearity into account is helpful for the compression of dissipative solitons, as a smaller minimum pulse width can be obtained, which suggests that a fiber segment is better than grating pairs or prism pairs for dissipative solitons' dechirping. A fluctuation after the minimum pulse width is obtained as shown in Fig. 7. This is due to the calculation program as we take the first peak for the pulse width calculation and the main peak of the dissipative soliton is compressed accompanied with pulse wing rising as shown in Figs. 7(a) (Media 1) and 7(b) (Media 2). Media 1 shows, for example, the pulse evolution in the 40-m-long SMF with the initial dissipative soliton obtained under the CPLDB of 1.6π and $G = 1000$, where the fiber nonlinearity is taken into account. Media 2 shows, for example, the pulse evolution in the 50-m-long SMF with the initial dissipative soliton obtained under the CPLDB of 1.6π and $G = 1000$, where the fiber nonlinearity is not taken into account. The nonlinear chirp of the dissipative soliton can be verified by the pedestal pulses generated around the main peak during pulse compression. Due to the large peak power of the compressed dissipative solitons, pulse breaking evolution can be observed after the pulse with minimum pulse width is achieved in both videos.

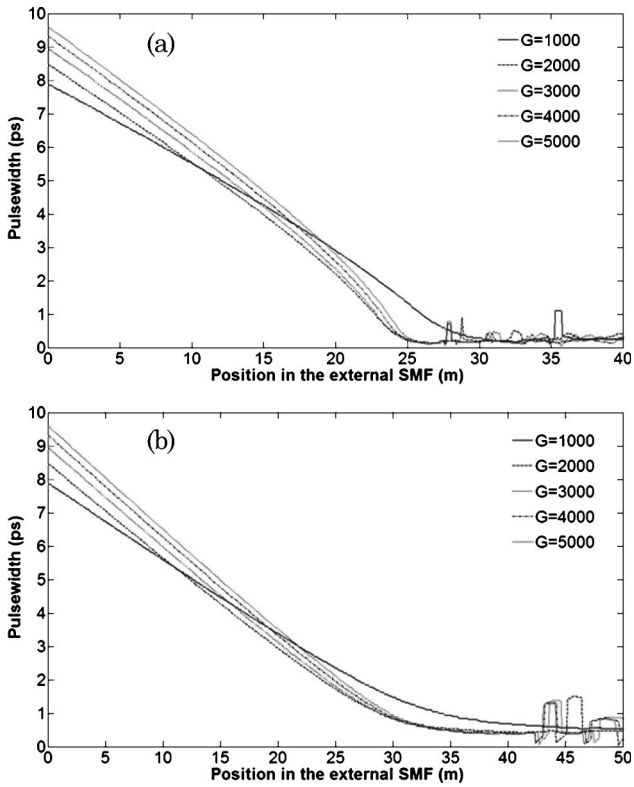

Fig. 7. Pulse width evolution in (a) a 40 m SMF with consideration of the fiber nonlinearity (Media 1) and (b) a 50 m SMF without consideration of the fiber nonlinearity (Media 2).

4. Conclusion

In conclusion, we have numerically studied the properties of dissipative solitons generated in all-normal-dispersion fiber lasers. We found that finite gain bandwidth is crucial for chirped pulse generation in fiber lasers operated in the NDR. The generated dissipative soliton is always heavily chirped. The frequency chirp of the generated dissipative soliton is increased with increasing pump power, and stronger pump power corresponds to faster instantaneous frequency variance. There exists an optimal pump value to achieve the maximum spectral bandwidth, which could be larger than the gain bandwidth limitation. Broader gain bandwidth can support a dissipative soliton with wider pulse width; therefore a gain medium with broader gain bandwidth can support a dissipative soliton with stronger pulse energy, provided the pump power is strong enough. Under the situation of maintaining the single pulse operation, strong pump power as large as

possible is useful for generating femtosecond pulses with high pulse energy, as the minimum pulse width could be obtained with a moderate length of SMF as a pulse compressor. Dissipative solitons are expected in YDF lasers without any intracavity discrete spectral filter. However, due to the broader spectral bandwidth of YDF and the limitation of the pump power of the available pump source for YDF lasers, no dissipative solitons have been observed. We believe that with the development of pump source technology, dissipative solitons can also be achieved in YDF lasers without any intracavity discrete spectral filter.

This work is supported by the Central Research Grant of the Hong Kong Polytechnic University under project G-YX0R. L. M. Zhao acknowledges the Singapore Millennium Foundation for providing him a postdoctoral fellowship in the Nanyang Technological University, Singapore.

References

1. J. Limpert, F. Roser, T. Schreiber, and A. Tunnermann, "High-power ultrafast fiber laser systems," IEEE J. Sel. Top. Quantum Electron. **12**, 233–244 (2006).
2. N. Akhmediev and A. Ankiewicz, eds., *Dissipative Solitons*, Lecture Notes in Physics (Springer, 2005), Vol. 661.
3. N. Akhmediev and A. Ankiewicz, eds., *Dissipative Solitons: From Optics to Biology and Medicine*, Lecture Notes in Physics (Springer, 2008), Vol. 751.
4. K. Tamura, E. P. Ippen, H. A. Haus, and L. E. Nelson, "77 fs pulse generation from a stretched-pulse mode-locked all-fiber ring laser," Opt. Lett. **18**, 1080–1082 (1993).
5. L. E. Nelson, S. B. Fleischer, G. Lenz, and E. P. Ippen, "Efficient frequency doubling of a femtosecond fiber laser," Opt. Lett. **21**, 1759–1761 (1996).
6. L. M. Zhao, D. Y. Tang, and J. Wu, "Gain-guided soliton in a positive group dispersion fiber laser," Opt. Lett. **31**, 1788–1790 (2006).
7. A. Chong, J. Buckley, W. Renninger, and F. Wise, "All-normal-dispersion femtosecond fiber laser," Opt. Express **14**, 10095–10100 (2006).
8. A. Cabasse, B. Ortaç, G. Martel, A. Hideur, and J. Limpert, "Dissipative solitons in a passively mode-locked Er-doped fiber with strong normal dispersion," Opt. Express **16**, 19322–19329 (2008).
9. L. M. Zhao, D. Y. Tang, H. Zhang, T. H. Cheng, H. Y. Tam, and C. Lu, "Dynamics of gain-guided solitons in an all-normal-dispersion fiber laser," Opt. Lett. **32**, 1806–1808 (2007).
10. A. Chong, W. H. Renninger, and F. W. Wise, "Properties of normal-dispersion femtosecond fiber lasers," J. Opt. Soc. Am. B **25**, 140–148 (2008).
11. W. H. Renninger, A. Chong, and F. Wise, "Dissipative solitons in normal-dispersion fiber lasers," Phys. Rev. A **77**, 023814 (2008).
12. B. G. Bale, J. N. Kutz, A. Chong, W. H. Renninger, and F. W. Wise, "Spectral filtering for high-energy mode-locking in normal dispersion fiber lasers," J. Opt. Soc. Am. B **25**, 1763–1770 (2008).
13. D. Y. Tang, L. M. Zhao, B. Zhao, and A. Q. Liu, "Mechanism of multisoliton formation and soliton energy quantization in passively mode-locked fiber lasers," Phys. Rev. A **72**, 043816 (2005).
14. E. Podivilov and V. L. Kalashnikov, "Heavily-chirped solitary pulses in the normal dispersion region: new solutions of the cubic-quintic complex Ginzburg-Landau equation," JETP Lett. **82**, 467–471 (2005).
15. L. M. Zhao, D. Y. Tang, J. Wu, X. Q. Fu, and S. C. Wen, "Noise-like pulse in a gain-guided soliton fiber laser," Opt. Express **15**, 2145–2150 (2007).
16. L. M. Zhao, D. Y. Tang, T. H. Cheng, H. Y. Tam, and C. Lu, "Generation of multiple gain-guided solitons in a fiber laser," Opt. Lett. **32**, 1581–1583 (2007).